Stability of the Matrix-Numerov Method for Solving 1D Schrödinger Equations

bachelor's thesis

presented by

Ole Jasper

Submitted to the Faculty of Mathematics, Computer Science and Natural Sciences of RWTH Aachen

under the supervision of

Prof. Dr. Fabian Hassler

Institute for Quantum Information

August 4, 2017

Contents

1 Introduction **1**
- 1.1 Motivation . . . 1
- 1.2 Chapter Overview . . . 1
- 1.3 Implementation . . . 2

2 Theoretical Foundation **3**
- 2.1 Discretization of Real Space . . . 3
- 2.2 Approximation of the Second-Order Derivative . . . 3
- 2.3 Numerov's Method . . . 5
- 2.4 Shooting Method . . . 6

3 Introduction of Matrix Methods **11**
- 3.1 Standard Matrix Method . . . 11
- 3.2 Matrix-Numerov Method . . . 12
- 3.3 Alternative Matrix Methods . . . 13

4 Application I: Cosine Potential **17**
- 4.1 Periodic Potential and Bloch's Theorem . . . 17
- 4.2 Calculation of Exact Solutions . . . 18
- 4.3 Numerical Evaluation . . . 19
- 4.4 Momentum Basis . . . 22

5 Application II: Coulomb Potential **25**
- 5.1 Hydrogen Atom . . . 25
- 5.2 Calculation of Exact Solutions . . . 26
- 5.3 Numerical Evaluation . . . 26

6 Conclusion **29**

7 Appendix **31**
- 7.1 Shooting Method with Numerov's Trick . . . 31

Bibliography **33**

Chapter 1

Introduction

1.1 Motivation

Since only a very limited set of physical problems yields an analytical solution for the Schrödinger equation, most applications in the field of quantum mechanics require numerical procedures to solve it. In order to apply those procedures as efficiently as possible, a good understanding of their behavior is necessary.

The matrix-Numerov method [1] is a modification of another more precedented way of approaching the time independent Schrödinger equation. In this thesis we want to compare it with other numerical methods, especially in regards to instability, which is known to be a key issue for some solving algorithms. Instability refers to any kind of behavior that results in a worsening or total divergence of the results where theory would suggest an improvement. In case one of them does not contain any instability problems it might offer advantages over other more commonly used methods. In this thesis we focus on the one dimensional Schrödinger equation to examine the behavior of different algorithms.

1.2 Chapter Overview

Before the introduction of any solving methods for Schrödinger equations, a mathematical basis has to be established in Ch. 2. This includes an explanation of the discretization of real space and the consequential way of approximating the second-order derivative operator. After constructing a generalized expression for the second-order derivative, Numerov's trick is introduced. We use it to improve the generalized second-order derivative operator.

Afterwards, we look at the Shooting Method as an example for a non-matrix method that inherits the generalized second-order derivative and use it to solve a simple problem. The occurring problems with this approach reveal the underlying key problem of instability directly resulting from the usage of the discretized second-order derivative. Therefore an incentive is given to move on from non-matrix methods to matrix methods. By doing so, we hope to find out whether they share the tendency towards instability or whether they offer a way to avoid it. In Ch. 3 four different matrix method are introduced, beginning with solving the eigenvalue problem by diagonalization of the Hamiltonian in real space. Following a similar approach, a matrix-Numerov method is derived by integrating Numerov's trick, yielding an improved matrix method. Two

more methods are presented at the end of Ch. 3.

These four methods are then tested in two separate practical applications in order to compare them quantitatively. The first application is a periodic cosine potential in Ch. 4, the second one a Coulomb potential in Ch. 5. Afterwards, a conclusion on which methods deliver the most precise and most stable results for each application is drawn in Ch. 6.

1.3 Implementation

All results generated in the course of this thesis stem from code implementations with `Python 2.7`. However, this thesis tries to treat each solving method as generically as possible, thus all results should be applicable to other platforms and forms of implementation. Whenever the exact python routine that was used might have impacted the results, it is mentioned explicitly.

Chapter 2

Theoretical Foundation

2.1 Discretization of Real Space

Before deriving matrix methods for solving the 1D Schrödinger equation, first some basic principles of numerical mathematics have to be discussed.
The foremost difference between analytical and most numerical approaches is the necessity to discretize real space. Throughout this thesis, the majority of numerical methods require a grid representation of real space. Whenever a quantity is represented by an equidistant grid with spacing a, the i-th point is referred to by using the notation

$$x_i = ia. \tag{2.1}$$

This also applies to quantities like the wave function $\psi_i = \psi(ia)$ or its derivatives $\psi_i^{(2)} = \psi^{(2)}(ia)$.

2.2 Approximation of the Second-Order Derivative

For most of the numerical methods we intent to examine, a discrete second-order derivative operator is required. On an evenly spaced grid, the common way to approximate the second-order derivative of a wave function $\psi(x)$ is the calculation of the difference quotient

$$\psi^{(2)}(x) = \frac{\psi(x-a) - 2\psi(x) + \psi(x+a)}{a^2} + \mathcal{O}\left(a^2\right). \tag{2.2}$$

This is the lowest order approximation of $\psi^{(2)}(x)$, from here on denoted as $r = 1$ as it only couples the next-neighbor elements at distance a. Higher order approximations can be achieved by increasing the number of wave function values on each side. In general, using $1+2r$ points (r points at each side in addition to the point at which the value of the second-order derivative is calculated) yields an approximation with an error of order $\mathcal{O}(a^{2r})$.

To obtain these higher order expressions, we look at the Taylor expansion of $\psi(x)$ in λ [2]

$$\psi(x \pm \lambda) = \psi(x) \pm \frac{\lambda}{1!}\psi^{(1)}(x) + \frac{\lambda^2}{2!}\psi^{(2)}(x) \pm \frac{\lambda^3}{3!}\psi^{(3)}(x) + ... \tag{2.3}$$

Since the terms of odd orders carry a sign dependent of the algebraic sign of $\pm\lambda$, adding the expansions $\psi(x+\lambda)$ and $\psi(x-\lambda)$ eliminates all odd-order terms. This reduced expansion of even order terms

$$\psi(x-\lambda)+\psi(x+\lambda)=2\psi(x)+2\frac{\lambda^2}{2!}\psi^{(2)}(x)+2\frac{\lambda^4}{4!}\psi^{(4)}+... \tag{2.4}$$

can be summarized as

$$\psi(x-\lambda)+\psi(x+\lambda)=\sum_{n=0}^{\infty}2\frac{\lambda^{2n}}{(2n)!}\psi^{(2n)}(x). \tag{2.5}$$

Stopping the expansion at $n=r$ and evaluating Eq. (2.5) for $\lambda=ja$ with $j\in\{-r,...,r\}\setminus\{0\}$ generates r independent equations [3]. Solving this system of equations yields the desired expression

$$\psi_i^{(2)}=\frac{1}{a^2}\sum_{j=-r}^{r}c_j\psi_{(i+j)}+\mathcal{O}\left(a^{2r}\right) \tag{2.6}$$

with the coefficients

$$c_j=\begin{cases}\frac{2(-1)^{j+1}(r!)^2}{j^2(r-|j|)!(r+|j|)!} & j\neq 0\\ \\ -2\sum_{k=1}^{r}\frac{1}{k^2} & j=0\end{cases} \tag{2.7}$$

where $\psi_{(i+j)}=\psi\left(x_{(i+j)}\right)=\psi((i+j)a)$ refers to the j-th neighbor of ψ_i. In addition to the generalized expression for the discretized second-order derivative, solving the system of equations can lead to a generalized expression for the $2r$-th derivative [4]

$$\psi_i^{(2r)}=\frac{1}{a^{2r}}\sum_{j=-r}^{r}d_j\psi_{(i+j)}+\mathcal{O}\left(a^2\right) \tag{2.8}$$

with the coefficients

$$d_j=(-1)^{j+r}\binom{2r}{r-|j|}. \tag{2.9}$$

While this expression is not required for the discretized second-order derivative itself, we are going to need it in the next section.

2.3 Numerov's Method

Numerov's Method is a numerical method to solve differential equations of the form

$$\psi^{(2)}(x) = -f(x)\psi(x) + s(x). \tag{2.10}$$

We want to use it to improve the accuracy of the expansion Eq. (2.6) by 2 orders of magnitude in the grid spacing a without including any additional lattice points. This is done by making use of the structure of the differential Eq. (2.10).

First, we rearrange the time independent Schrödinger equation

$$\left[-\frac{\hbar^2}{2m}\frac{\partial^2}{\partial x^2} + V(x)\right]\psi(x) = E\psi(x) \tag{2.11}$$

into the form

$$\psi^{(2)}(x) = -\frac{2m}{\hbar^2}\left[E - V(x)\right]\psi(x). \tag{2.12}$$

Eq. (2.12) now fulfills the requirement from Eq. (2.10) with

$$f(x) = \frac{2m}{\hbar^2}\left[E - V(x)\right],\ s(x) = 0. \tag{2.13}$$

Therefore the Schrödinger equation is suitable for being solved with Numerov's Method. In order to improve the accuracy, the expansion in Eq. (2.5) derived in the last section is stopped at $n = r + 1$ rather than at $n = r$ to include the term of order $\mathcal{O}\left(a^{2r}\right)$. Afterwards, this expression is solved for the unknown $\psi^{(2n)}(x)$ again, while retaining $\psi^{(2r+2)}(x)$ as a free parameter [4].

Similarly to Eq. (2.6), this yields an expression for the discretized second-order derivative of $\psi(x)$

$$\begin{aligned}\psi_i^{(2)} = \frac{1}{a^2}\sum_{j=-r}^{r} c_j\psi_{(i+j)} + a^{2r}\frac{(-1)^{r+1}(r!\,)^2}{(2r+1)!\,(r+1)} \\ \times \sum_{j=-r}^{r}\psi_i^{(2r+2)} + \mathcal{O}\left(a^{2r+2}\right).\end{aligned} \tag{2.14}$$

Now, we have increased the order of the error from $\mathcal{O}\left(a^{2r}\right)$ to $\mathcal{O}\left(a^{2r+2}\right)$ by including an additional term of the Taylor expansion. Unfortunately the current form is not usable yet, since $\psi_i^{(2r+2)}$ is not known. This is where Numerov's trick comes into play by exploiting the structure of the differential equation. Acting on both sides of Eq. (2.10) with ∂_x^{2r}, assuming $s(x) = 0$, we obtain the

equation

$$\psi^{(2r+2)}(x) = -\left(\partial_x\right)^{2r}\left[f(x)\psi(x)\right] \tag{2.15}$$

and plug it into Eq. (2.14). Afterwards $\psi^{(2r)}(x)$ can be substituted with Eq. (2.8) from the previous section resulting in an improved version of the discretized second-order derivative

$$\begin{aligned}\psi_i^{(2)} = &\frac{1}{a^2}\sum_{j=-r}^{r} c_j\psi_{(i+j)} \\ &+ \frac{(-1)^{r+1}(r!\,)^2}{(2r+1)!\,(r+1)}\sum_{j=-r}^{r} d_j f_{(i+j)}\psi_{(i+j)} + \mathcal{O}\left(a^{2r+2}\right).\end{aligned} \tag{2.16}$$

2.4 Shooting Method

While the discretized second-order derivative can be used for a variety of methods to solve 1D Schrödinger equations, often instability issues become a problem. For both approximations - either with or without Numerov's trick - the occurrence of instabilities seems to correlate directly with the order r [5].This can be illustrated by a short look at the shooting method. This short digression serves the comprehensibility of instability issues; the shooting method will not be of any interest subsequently.

The shooting method is a numerical solving method for boundary value problems of the form

$$\psi^{(2)}(x) = g\left(x,\ \psi(x),\ \psi^{(1)}(x)\right),\ \psi(x_0) = \psi_0,\ \psi(x_N) = \psi_N, \tag{2.17}$$

with $g = \frac{2m}{\hbar^2}\left[V(x) - E\right]\psi(x)$ in this case. For solving the Schrödinger equation, we introduce a wave function $\psi(x, E)$ which has the system's energy E as a parameter. The method's name stems from the procedure of guessing an initial value for E, 'shooting' a trajectory, and then examining how well it fulfills the boundary condition $\psi(x_N) = \psi_N$, thereby determining the quality of E.

Shooting the trajectory $\psi(x, E)$ for a certain value of E can be realized with the Runge-Kutta method [6] by utilizing the discretized second-order derivative operator. While this can also be done with its Numerov-improved version from Eq. 2.16 , it is demonstrated here without it, simply because this way the expansion includes one term less, resulting in a more comprehensible iteration formula. However, the same procedure with Numerov's trick can be found in the App. 7.1. Plugging the generalized second-order derivative from Eq. (2.6)

into the Schrödinger equation yields

$$\frac{1}{a^2}\sum_{j=-r}^{r} c_j\psi_{(i+j)} + \mathcal{O}\left(a^{2r}\right) = \frac{2m}{\hbar^2}\left[V_i - E\right]\psi_i. \tag{2.18}$$

Excluding the last term $j = r$ from the sum and rearranging this expression results in a recursive expression for $\psi_{(i+r)}$

$$\psi_{(i+r)} = \frac{1}{c_r}\left(\frac{2m}{\hbar^2}a^2\left[V_i - E\right]\psi_i - \sum_{j=-r}^{r-1} c_j\psi_{(i+j)}\right). \tag{2.19}$$

When $2r$ consequent values of the wave function are known, this formula allows the calculation of the next value as illustrated in Fig. 2.1. By incrementing i successively, wave function values at all lattice points can be generated.

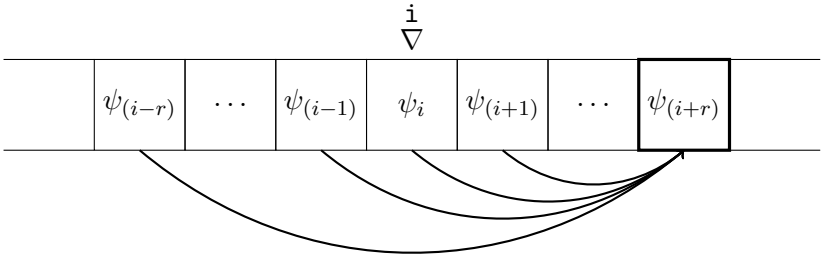

Figure 2.1: Calculation of the $(i+r)$-th value of the wave function using the $2r$ values on its left. This illustrates one step of the Runge-Kutta iteration process to obtain wave function values at all lattice points.

As the last point ψ_N is calculated, it can be compared to the boundary condition from Eq. (2.17) to evaluate the quality of the initially guessed eigenenergy E. Combining this approach with a bisection algorithm by guessing two energies $E^{(l)} < E < E^{(h)}$ initially, shooting a trajectory for each one, determining which one is closer to E, and reducing the interval accordingly, successively approximates E.

One possible implementation of a shooting method to determine an eigenenergy E_n is shown in Alg. 1.

Algorithm 1
Shooting method to determine $E = E_n$ through bisection

procedure
set $E^{(l)}$ and $E^{(h)}$ around E
$E^{(c)} \leftarrow \left(E^{(l)} + E^{(h)}\right)/2$

/* Loop while energy interval is bigger than $size$ */
while$(E^{(h)} - E^{(l)} > size)$
    /* Too many zero-crossings in $\psi^{(c)}$ */
    if $(\text{knots}\left(\psi^{(c)}\right) > n)$ **then**
        $E^{(h)} \leftarrow E^{(c)}$
    /* Not enough zero-crossings in $\psi^{(c)}$ */
    if $(\text{knots}\left(\psi^{(c)}\right) < n)$ **then**
        $E^{(l)} \leftarrow E^{(c)}$
    /* Eigenenergy E lies between $E^{(l)}$ and $E^{(c)}$ */
    if $(\text{compare\_boundary}\left(\psi^{(l)}\right) * \text{compare\_boundary}\left(\psi^{(c)}\right) < 0)$ **then**
        $E^{(h)} \leftarrow E^{(c)}$
    /* Eigenenergy E lies between $E^{(c)}$ and $E^{(h)}$ */
    if $(\text{compare\_boundary}\left(\psi^{(c)}\right) * \text{compare\_boundary}\left(\psi^{(h)}\right) < 0)$ **then**
        $E^{(l)} \leftarrow E^{(c)}$
    $E^{(c)} \leftarrow \left(E^{(l)} + E^{(h)}\right)/2$

return $E^{(c)}$

In Alg. 1 $E^{(l)}$ and $E^{(h)}$ describe the energies surrounding E. Their arithmetic mean is $E^{(c)}$ and each energy's wave function generated using the Runge-Kutta method is labeled accordingly.
The function `knots()` returns the number of zero-crossings of the corresponding wave function, `compare_boundary()` returns the difference between the boundary condition value ψ_N and the last value of the wave function it is used on. In case two wave functions have the correct amount of zero-crossings, the product of what `compare_boundary()` returns when used on them indicates whether E lies between their associated energies. If their product is negative, one wave function ends to high and the other one too low, therefore the solution is somewhere between them. As soon as the energy interval $E^{(h)} - E^{(l)}$ is smaller than the given $size$, $E^{(c)}$ is returned as the solution.

In order to illustrate that using orders $r > 1$ in the Runge-Kutta method results in issues, we use the bisection algorithm Alg. 1 to determine the ground state energy of a particle in a box with

$$V(x) = \begin{cases} 0, & 0 < x < 2\pi \\ \infty, & \text{else} \end{cases} \tag{2.20}$$

and the discretized real space

$$x_i = ia,\ i \in [0, N]\,,\ a = \frac{2\pi}{N}. \tag{2.21}$$

We identify the underlying boundary value problem as

$$\psi^{(2)}(x) = \frac{2m}{\hbar^2}\left[V(x) - E\right]\psi(x),\ \psi(0) = 0,\ \psi(2\pi) = 0. \tag{2.22}$$

Since we know the exact ground state energy $E_1 = \hbar^2\pi^2/2m(L)^2 = \hbar^2/8m$ from theory, we chose $E^{(l)}$ and $E^{(h)}$ slightly below and above it, and determine E_1 using the shooting method as depicted in Fig. 2.2. The first order $r = 1$ approximation is used in the Runge-Kutta method from Eq. (2.19).

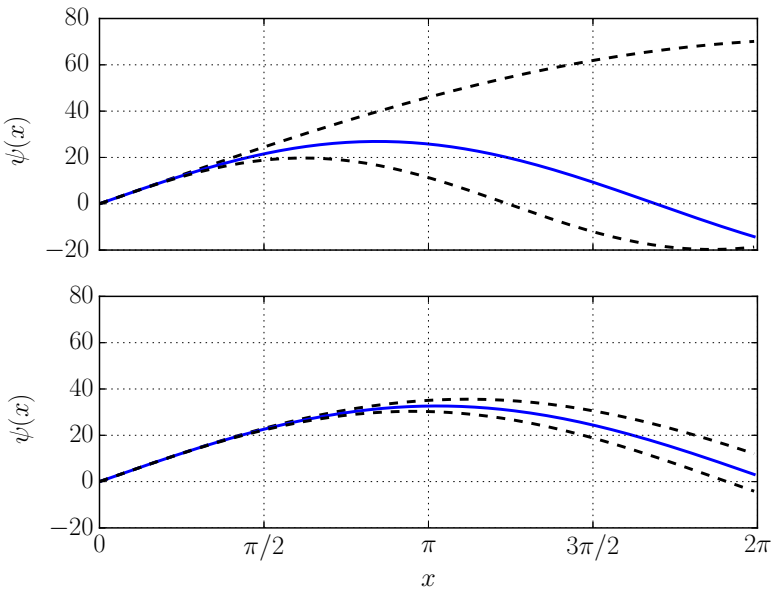

Figure 2.2: Ground state wave function of a particle in a box approximated with Alg. 1. The first blue graph shows $\psi^{(c)}$ after 0, the second one after 3 steps of bisection. The dashed lines depict the wave functions generated from the current lower and upper energy interval limits $E^{(l)}$ and $E^{(h)}$. For shooting the trajectories the Runge-Kutta method Eq. (2.19) in order $r = 1$ on $N = 200$ lattice points was used.

Repeating the process of calculating the ground state energy for different numbers of lattice points N indicates how the result benefits from increasing N (see Tab. 2.1. Results with Numerov's trick can be found in App. 7.1).

N	200	400	800	1600	3200	6400
$\Delta E_1/E_1$	1.00e-02	5.04e-03	2.48e-03	1.23e-03	6.47e-04	2.81e-04

Table 2.1: Relative errors of ground state energy $\Delta E_1/E_1 = \left|E_1 - E^{(c)}\right|/E_1$ calculated with the bisection Alg. 1 for different numbers of lattice points N. A higher number of lattice points results in a direct improvement of the result.

However, when a higher order $r > 1$ approximation of the second-order derivative is used in the Runge-Kutta method, the wave function diverges, causing the entire shooting method to fail. This also happens when using the Numerov-improved version. Therefore the shooting method is restricted to using the first order approximation only.

Since the matrix methods we introduce in Ch. 3 evolve around different orders r of approximation, we want to examine whether instability is a problem inherent to the Runge-Kutta method or if different approaches share this issue somehow. The approximations of the second-order derivative operator in Eq. (2.6) and its Numerov-improved version in Eq. (2.16) benefit greatly from increasing r, therefore solving methods which can make use of higher orders r would be advantageous.

Chapter 3

Introduction of Matrix Methods

3.1 Standard Matrix Method

An important reason to move on from the shooting method is the rise of its run time for an increasingly large number of lattice points N, because the combination of the bisection method with the Runge-Kutta method results in a high number of iterations over every point in real space. In opposition to that, an approach with matrix methods allows finding multiple eigenenergies of the particular problem simultaneously and much faster.

In addition to that, we suspect matrix methods to be capable of using higher order approximations $r > 1$. If this proves to be true, higher orders can be used to achieve more accurate results.

The idea of the first matrix-method we introduce is a direct result of the equidistant grid representation of real space with lattice spacing a. Due to the vector-like structure of both real space and the projection of the wave function $\psi(x)$ onto it, the Schrödinger equation

$$H\psi = E\psi \tag{3.1}$$

turns into an eigenvalue problem with $H \in \mathbb{R}^{N\times N}$. The eigenenergies can therefore be contained by finding the eigenvalues of the real space matrix representation of the Hamiltonian H, with the wave functions as the corresponding eigenvectors.

Diagonalizing the Hamiltonian in real space primarily requires finding a diagonal matrix representation of the kinetic energy T, since the potential energy matrix

$$\langle i| V |i\rangle = V_i = V(ia) \tag{3.2}$$

is already diagonal. For the kinetic energy matrix on the other hand, we can utilize the discretized second-order derivative

$$\psi_i^{(2)} = \frac{1}{a^2} \sum_{j=-r}^{r} c_j \psi_{(i+j)} + \mathcal{O}\left(a^{2r}\right). \tag{3.3}$$

The summation over the lattice points contributing to the second-order derivative of each point corresponds to matrix elements on the off-diagonals $-r$ to r. This means the j-th diagonal of T has the value c_j/a^2 for $j \in [-r, r]$ multiplied with the prefactors from the Schrödinger equation.

For $r = 1$ we obtain

$$T = -\frac{\hbar^2}{2m}\frac{1}{a^2}\begin{pmatrix} c_0 & c_1 & 0 & \cdots & 0 \\ c_1 & c_0 & c_1 & \ddots & \vdots \\ 0 & \ddots & \ddots & \ddots & 0 \\ \vdots & \ddots & c_1 & c_0 & c_1 \\ 0 & \dots & 0 & c_1 & c_0 \end{pmatrix} \tag{3.4}$$

As we can see $(2r + 1) \leq N$ has to be fulfilled at all times. Furthermore when determining the eigenvalues of $H = T + V$ numerically, we have to consider under which circumstances the occurring matrices are sparse. When sparse matrices are solved for their eigenvalues, special sparse matrix methods are more efficient than standard matrix methods.
Since a matrix is sparse if the number of matrix elements unequal to zero n is small compared to the total number of elements $N \times N$ and V has a maximum of N non-zero entries, the overall sparsity of the Hamiltonian depends entirely on the sparsity of the kinetic energy matrix T. Because c_j never becomes zero and the j-th diagonal has the length $N - j$, the total number of entries unequal to zero is

$$n = \sum_{j=-r}^{r} (N - |j|) = N + 2\sum_{j=1}^{r} (N - j) = N(2r + 1) - r\,(r + 1)\,. \tag{3.5}$$

Thereby we have derived the requirement

$$N(2r + 1) - r\,(r + 1) \ll N \times N \tag{3.6}$$

for any order r that still maintains the sparsity of the Hamiltonian.

3.2 Matrix-Numerov Method

In a very similar fashion to the standard matrix method, the discretized second-order derivative including Numerov's trick can be employed to derive a matrix

method. However, since this expression for the second-order derivative

$$\begin{aligned}\psi_i^{(2)} = &\frac{1}{a^2}\sum_{j=-r}^{r} c_j \psi_{(i+j)} \\ &+ \frac{(-1)^{r+1}(r!)^2}{(2r+1)!\,(r+1)} \sum_{j=-r}^{r} d_j f_{(i+j)} \psi_{(i+j)} + \mathcal{O}\left(a^{2r+2}\right)\end{aligned} \tag{3.7}$$

contains elements of the potential energy matrix in $f_{(i+j)} = 2m/\hbar^2 \left[E - V_{(i+j)}\right]$, the Hamiltonian cannot simply be diagonalized by separating it into a kinetic and a potential energy term as before. Expanding the Numerov-improved approximation of the second-order derivative into

$$\begin{aligned}\psi_i^{(2)} = &\frac{1}{a^2}\sum_{j=-r}^{r} c_j \psi_{(i+j)} + E\frac{2m}{\hbar^2}\frac{(-1)^{r+1}(r!)^2}{(2r+1)!\,(r+1)} \sum_{j=-r}^{r} d_j \psi_{(i+j)} \\ &- V\frac{2m}{\hbar^2}\frac{(-1)^{r+1}(r!)^2}{(2r+1)!\,(r+1)} \sum_{j=-r}^{r} d_j \psi_{(i+j)},\end{aligned} \tag{3.8}$$

and plugging it into the Schrödinger equation yields

$$\left[V - \frac{\hbar^2}{2m}A - EB + VB\right]\psi(x) = E\psi(x), \tag{3.9}$$

the matrices A with c_j/a^2, and B with $[d_j(-1)^{r+1}(r!)^2]/[(2r+1)!\,(r+1)]$ on their j-th diagonals. Rearranging this into the form of a generalized eigenvalue problem provides the equation

$$\left[-\frac{\hbar^2}{2m}A + (B+1)V\right]\psi(x) = (B+1)E\psi(x). \tag{3.10}$$

With the same argumentation as for the matrix method without Numerov's trick, the criteria for sparsity Eq. (3.6) still applies and therefore when fulfilled allows using sparse matrix functions efficiently.

3.3 Alternative Matrix Methods

In addition to the standard matrix and the matrix-Numerov method, we want to introduce two alternative matrix methods following a different approach. Both of them start off by writing the Schrödinger equation as a generalized eigenvalue problem

$$-\frac{\hbar^2}{2m}\underbrace{B^{-1}A}_{\partial_x^2}\psi(x) = (E - V)\psi(x) \tag{3.11}$$

and finding expressions for matrices A and B, so that $B^{-1}A$ approximates the second-order derivative acting on $\psi(x)$. To achieve this, we we take a look at the basis functions

$$\psi^k(x) = e^{ikx}, \text{ with } k \in [-\pi, \pi). \tag{3.12}$$

The effect of the second-order derivative on them is $\partial_x^2 \psi^k(x) = -k^2 \psi^k(x)$. Therefore in order for the matrices A and B to approximate the second-order derivative, they must approximate $-k^2$

$$\frac{A\psi^k(x)}{B\psi^k(x)} \approx -k^2. \tag{3.13}$$

For this derivation we choose lattice spacing $a = 1$. Similarly to Sec. 3.1 through the discretization of real space the effect of each matrix acting on $\psi^k(x)$ is defined by their diagonal elements a_j and b_j

$$A\psi^k(x) = \sum_{j=-r}^{r} a_j e^{ikj}, \; B\psi^k(x) = \sum_{j=-r}^{r} b_j e^{ikj}. \tag{3.14}$$

In combination with Eq. (3.13), this yields

$$f(k) = \frac{\sum_{j=-r}^{r} a_j e^{ikj}}{\sum_{j=-r}^{r} b_j e^{ikj}} \approx -k^2. \tag{3.15}$$

Now, the matrix elements a_j and b_j can be determined analytically to approximate $-k^2$ for different orders r as illustrated in Fig. 3.1. Afterwards we can fill the j-th diagonal of A with a_j/a^2, where a denotes the actual grid spacing of real space, the j-th diagonal of B with b_j, and solve

$$\left[BV - \frac{\hbar^2}{2m} A\right] \psi(x) = BE\psi(x) \tag{3.16}$$

with standard routines for the generalized eigenvalue problem.

An additional method can be extracted with a slight alteration. The idea is to let our approximation of $-k^2$ diverge at $k = \pm\pi$. To do so, we reserve one b_j and use it to cause the divergence at $k = \pm\pi$ illustrated in Fig. 3.2. While this reduces the precision of our approximation in total, it is worth to examine whether this modified alternative matrix method is superior. Besides the alteration of the coefficients b_j, the general procedure of solving the generalized eigenvalue problem in Eq. (3.16) stays identical.

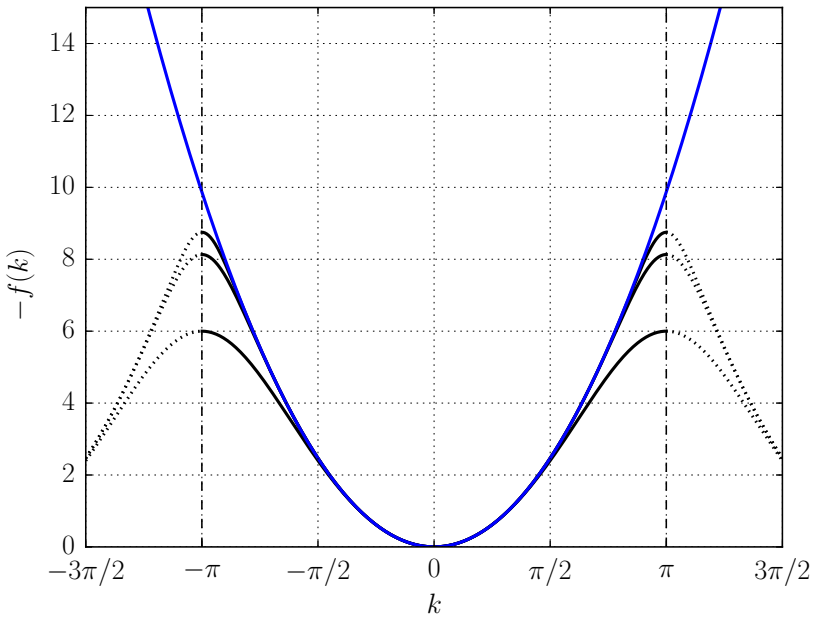

Figure 3.1: Approximations of $-k^2$(blue) by $-f(k)$ from Eq. (3.15) with $r = 1, 3, 5$. Each graph's behavior outside of $|k| < \pi$ is continued with dashed lines.

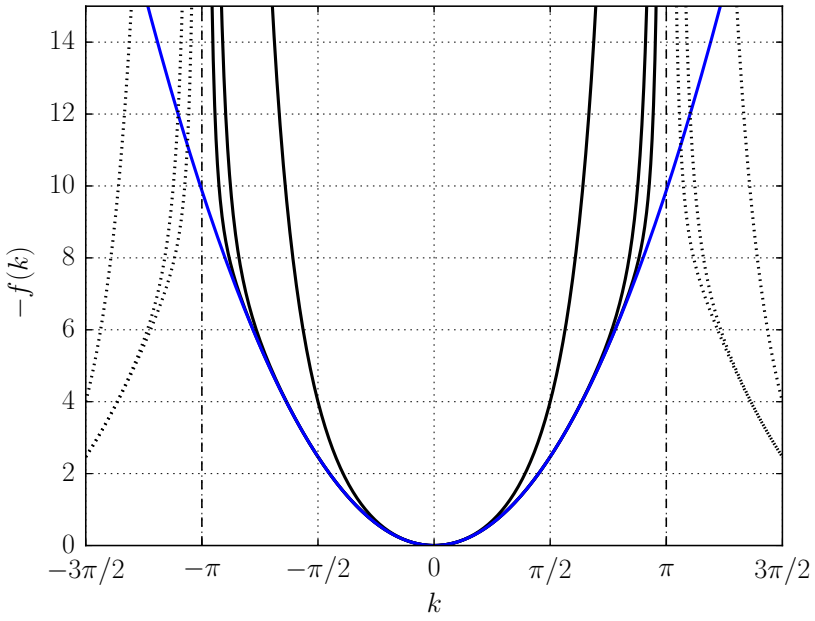

Figure 3.2: Approximations of $-k^2$(blue) by $-f(k)$ from Eq. (3.15) with $r = 1, 3, 5$ and with divergence at $k = \pm\pi$. Each graph's behavior outside of $|k| < \pi$ is continued with dashed lines.

Now that we introduced four solving methods

1. Standard matrix method (from Sec. 3.1)
2. Matrix-Numerov method (from Sec. 3.2)
3. Alternative matrix method (from Sec. 3.3)
4. Alternative matrix method with divergence (from Sec. 3.3),

we want to compare them by evaluating two separate problems. A special emphasis lies on whether using higher orders r results in instability. Furthermore we intend to find out which method generates the best result for each particular problem.

Chapter 4

Application I: Cosine Potential

4.1 Periodic Potential and Bloch's Theorem

Even though our the matrix methods can be applied for any given potential in theory, there are a few conditions that have to be met in order to conduct a meaningful examination. First and foremost the solution's wave function needs to be representable on a finite regime of real space. This works if the wave function becomes arbitrarily small on a global scale except for a limited interval that then might be described by a grid. However, in this case we introduce the periodic cosine-potential illustrated in Fig. 4.1.

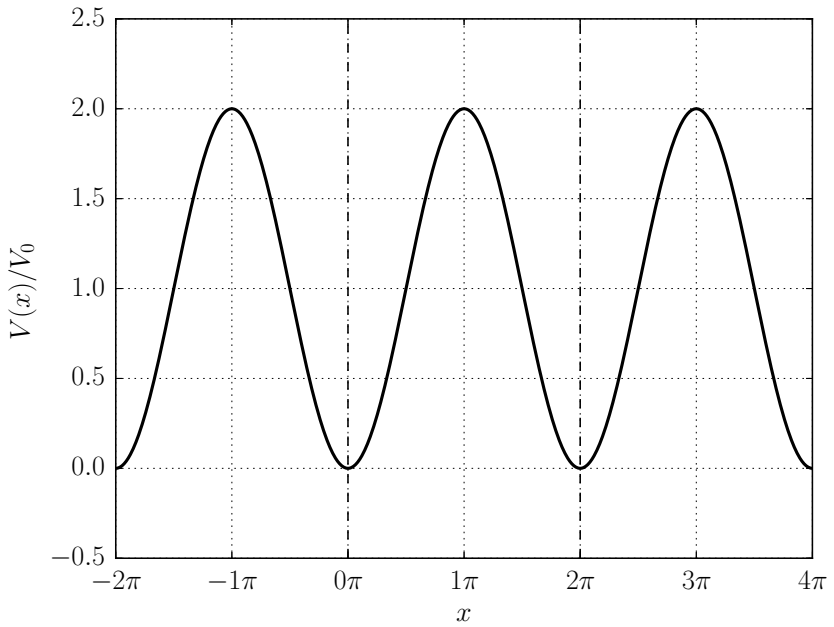

Figure 4.1: Cosine potential $V(x) = V_0(1 - \cos(x))$.

According to Bloch's Theorem the 2π-periodicity of the potential $V(x)$

$$V(x + 2\pi) = V(x) \tag{4.1}$$

directly implies a 2π-periodicity of the wave functions $\psi(x)$ that solve the Schrödinger equation

$$\psi(x + 2\pi) = \psi(x). \tag{4.2}$$

Therefore the entire problem may be described on an interval between 0 and 2π with a lattice of N points

$$x_i = ia,\ i \in [0, N-1] \tag{4.3}$$

with equidistant lattice spacing $a = 2\pi/N$. We intentionally exclude $x_N = Na$, since the lattice point at $x = 0$ corresponds to $x = 2\pi$, due to the periodic boundary condition Eq. (4.2). Knowing the spatial extent of real space leaves N as the only free parameter, allowing us to examine its direct impact on the quality of each method.

4.2 Calculation of Exact Solutions

In order to compare the different solving methods, we determine the cosine problem's eigenenergies analytically. Since the constant offset V_0 in the Hamiltonian only results in an offset on the eigenenergies, we can add it to the solutions at the end and exclude it for now. This way the reduced Schrödinger equation

$$\left[-\frac{\hbar^2}{2m}\frac{\partial^2}{\partial x^2} - V_0\cos(x)\right]\psi(x) = E\psi(x) \tag{4.4}$$

can be recast into the form of a standard Mathieu problem [7]

$$y'' + [a - 2q\cos(2x)]\, y = 0. \tag{4.5}$$

We obtain the differential equation

$$\psi''(x) + \left[-\frac{8Em}{\hbar^2} + \frac{8V_0 m}{\hbar^2}\cos(2x)\right]\psi(x) = 0 \tag{4.6}$$

and identify $a = -8Em/\hbar^2$ and $q = -4V_0 m/\hbar^2$ to use the standard formula for solving the Mathieu problem. This yields the eigenenergies

$$E_n = \frac{\hbar^2}{8m} b_{2n}(q) + V_0, \tag{4.7}$$

where $b_\nu(q)$ denotes Mathieu's characteristic values. Since we subtracted V_0 from the Hamiltonian in the beginning, we now have to add V_0 to obtain the correct results.

4.3 Numerical Evaluation

To compare the four numerical methods quantitatively, we look at the relative error $\Delta E_1/E_1 = |E_1 - E_{1,\text{numerical}}|/E_1$ between the exact and the numerically found ground state energy. We generate this value with each method at an exponentially increasing number of lattice points N. Since all occurring matrices are sufficiently small, we use `scipy.sparse.linalg.eigsh` in the shift-invert mode to determine eigenvalues.

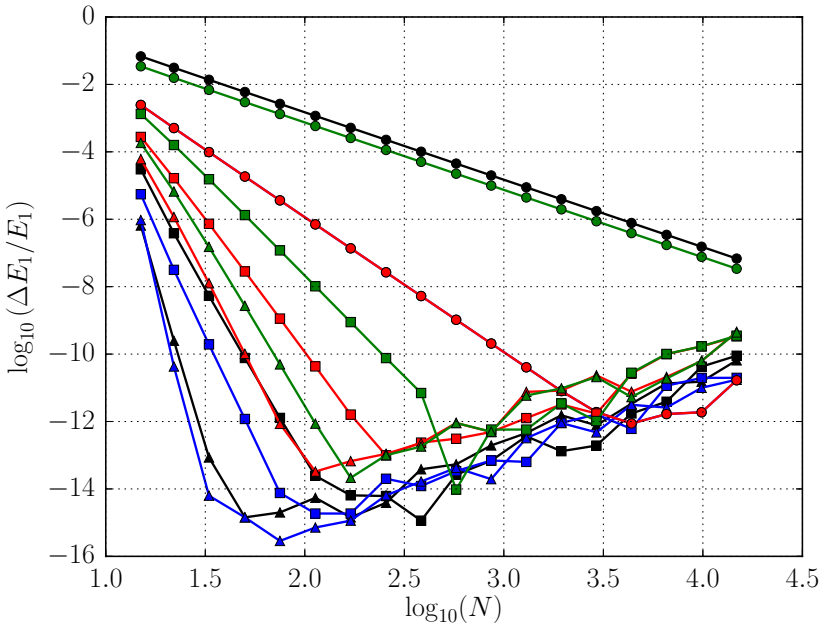

Figure 4.2: Comparison of all 4 matrix methods with $r = 1(\bigcirc)$, $3(\square)$, $5(\triangle)$ and a potential with $V_0 = 10$. Green: standard matrix method; Red: matrix-Numerov method; Blue: alternative matrix method; Black: alternative matrix method with divergence. Within each color, a higher order r results in a quicker convergence.

Between the graphs of the same method, depicted in the same color, the slope of each curve directly correlates with its order r. This confirms our expectation that using a higher order r results in a quicker convergence towards the exact eigenenergy.

However, all graphs appear to reach a minimum, with the exception of the standard matrix method with $r = 1$ and the alternative matrix method with divergence with $r = 1$. Thus those two methods do not converge fast enough to reach a regime in which they diverge. Since the graph of a stable solving method would maintain a constant value at machine precision around $\log_{10}(\Delta E_1/E_1) \approx -15$, the graphs' rise indicates some form of instability.
Those methods which share this behavior reach their minimum at a different

number of lattice points, depending on their initial slope. In general, the steeper a graph in its first linear regime, the lower its minimum and therefore the better its best result appears to be.

After reaching their minimum, each graph follows the same linear rise, that thereby constitutes a lower limit for all algorithms. We determine this function by regressions on the according linear regime of each graph whose results are shown in Tab. 4.1.

Method	**order** r	**slope**	**intercept**	χ^2_{dof}
Standard matrix method	1	-	-	-
Standard matrix method	3	2.94	-21.48	0.91
Standard matrix method	5	1.90	-17.60	0.92
Matrix-Numerov method	1	2.21	-20.23	0.81
Matrix-Numerov method	3	2.07	-18.23	0.95
Matrix-Numerov method	5	1.79	-17.17	0.94
Alt. Matrix method	1	2.21	-20.23	0.81
Alt. Matrix method	3	2.02	-19.01	0.95
Alt. Matrix method	5	2.11	-19.41	0.97
Alt. Matrix method w. divergence	1	-	-	-
Alt. Matrix method w. divergence	3	2.66	-21.33	0.92
Alt. Matrix method w. divergence	5	1.97	-18.59	0.96

Table 4.1: Results of linear regressions of all graphs in Fig. (4.2) on the regimes where they rise linearly. Since two of them do not incorporate a linear rise, they are excluded here.

Averaging the linear regressions in the second regime of each graph from Tab 4.1 yields an expression for the linear function $f(\log_{10}(N))$ depicted in Fig. 4.3, constituting the lower limit of all solving methods in Fig. 4.2

$$f(\log_{10}(N)) = (2.19 \pm 0.34)\log_{10}(N) - (19.33 \pm 1.41)\,. \tag{4.8}$$

The method which reaches the lowest minimum and provides the best result, is the alternative matrix method without divergence. Adding $r = 7$ to the plot as in Fig. 4.4, suggests that higher orders continue to deliver better results. In fact the graph of this method with $r = 7$ reaches machine precision before the graph intersects the linear lower limit from Eq. 4.8. Therefore a constant value at machine precision is held until the divergence begins.

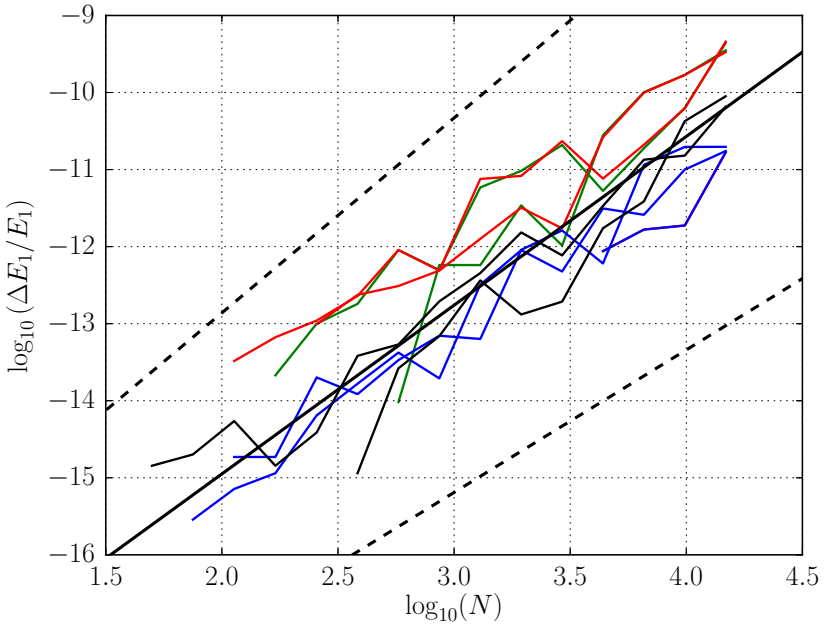

Figure 4.3: Approximate linear behavior from Eq. (4.8) depicted by the black line, derived from averaging the linear regressions in Tab. 4.1. The colored graphs describe the linear rise of each function from Fig. 4.2. The dashed black lines incorporate the statistical error of the averaged linear regression.

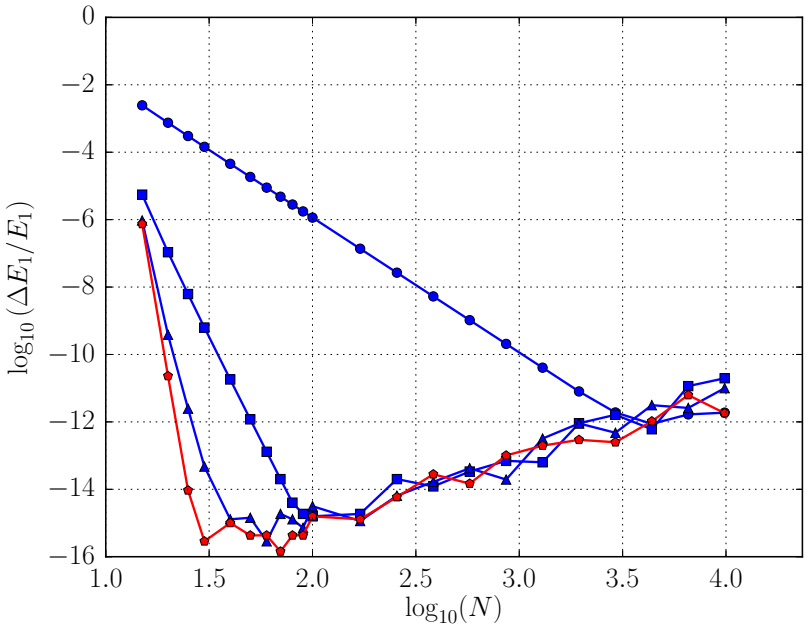

Figure 4.4: Alternative matrix method without divergence with $r = 1(\bigcirc)$, $3(\square)$, $5(\triangle)$, $7(\pentagon)$ and $V_0 = 10$ for different numbers of lattice points N. The highest order $r = 7$ is depicted in red. Before this particular graph starts to diverge, it manages to reach a plateau at machine precision.

4.4 Momentum Basis

Another way of calculating the eigenenergies is the diagonalization of the Hamiltonian in the momentum basis. Unlike the other matrix methods, this one is especially useful for periodic potentials. Since using this method is only used for this application and not for the Coulomb potential in Ch. 5, it is discussed separately here.

In opposition to the matrix representation of the Hamiltonian in real space, in the momentum basis $\langle x|\,|\phi_l\rangle = e^{ilx}/\sqrt{2\pi}$ the kinetic energy term is diagonal and a diagonalization of the potential energy matrix has to be found. To exploit the periodic nature of $V(x)$, we separate the cosine part of the Hamiltonian from the rest.

$$\langle\phi_l\,|\,H\,|\,\phi_k\rangle = \langle\phi_l|\underbrace{\left(V_0 - \frac{\hbar^2}{2m}\frac{\partial^2}{\partial x^2}\right)}_{=H_I}|\phi_k\rangle + \langle\phi_l|\underbrace{-V_0\cos(x)}_{=H_{II}}|\phi_k\rangle \tag{4.9}$$

Each term can be transformed independently by using the Fourier transformation.

$$\begin{aligned}\langle\phi_l\,|\,H_I\,|\,\phi_k\rangle &= \int e^{-ilx}\left(V_0 - \frac{\hbar^2}{2m}\frac{\partial^2}{\partial x^2}\right)e^{ikx}dx \\ &= \left(V_0 + \frac{\hbar^2}{2m}k^2\right)\int e^{i(k-l)x}dx \\ &= \left(V_0 + \frac{\hbar^2}{2m}k^2\right)\delta_{k,l}\end{aligned} \tag{4.10}$$

$$\begin{aligned}\langle\phi_l\,|\,H_{II}\,|\,\phi_k\rangle &= \int e^{-ilx}\left(-V_0\cos(x)\right)e^{ikx}dx \\ &= -V_0\int e^{-ilx}\frac{1}{2}\left(e^{ix}+e^{-ix}\right)e^{ikx}dx \\ &= -\frac{1}{2}V_0\int\left(e^{i(k-l+1)x}+e^{i(k-l-1)x}\right)dx \\ &= -\frac{1}{2}V_0\left(\delta_{l,k+1}+\delta_{l,k-1}\right)\end{aligned} \tag{4.11}$$

The transformation yields that the Hamiltonian in momentum basis is a matrix containing $\left(V_0 - \frac{\hbar^2}{2m}k^2\right)$ on its main diagonal and $-\frac{1}{2}V_0$ on its first upper and

lower off-diagonal.

$$\langle \phi_l \,|\, H \,|\, \phi_k \rangle = V_0 \begin{pmatrix} 1 & -\frac{1}{2} & 0 & \dots & 0 \\ -\frac{1}{2} & 1 & -\frac{1}{2} & \ddots & \vdots \\ 0 & \ddots & \ddots & \ddots & 0 \\ \vdots & \ddots & -\frac{1}{2} & 1 & -\frac{1}{2} \\ 0 & \dots & 0 & -\frac{1}{2} & 1 \end{pmatrix} \tag{4.12}$$
$$-\frac{\hbar^2}{2m} \begin{pmatrix} 1^2 & 0 & \dots & \dots & 0 \\ 0 & 2^2 & \ddots & \ddots & \vdots \\ \vdots & \ddots & \ddots & \ddots & \vdots \\ \vdots & \ddots & \ddots & (N-1)^2 & 0 \\ 0 & \dots & \dots & 0 & N^2 \end{pmatrix}$$

The dimension N of this matrix corresponds to the number of lattice points in momentum space.
When analyzing this method analogously to the others, it shows vastly superior results. Since it converges exponentially, we plot the relative error of the ground state energy against N in Fig 4.5. The graph's behavior up until its plateau at machine precision is reached confirms that this method converges exponentially instead of the polynomial convergence the other methods show. In addition to the quicker convergence, this method does not hint any sign of divergence for high N regardless of V_0. Therefore the momentum basis matrix method has to be considered vastly superior as far as this very problem is concerned.

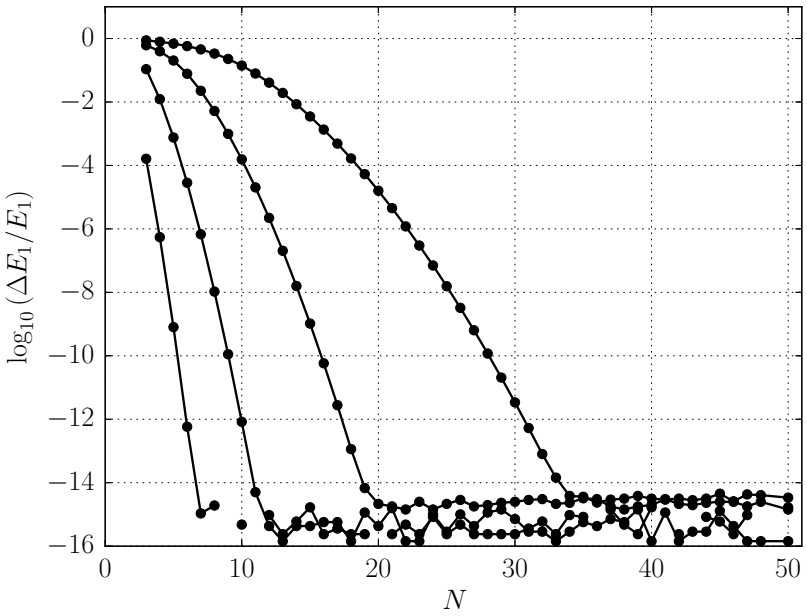

Figure 4.5: Exponential convergence of momentum basis matrix method for $V_0 = 1, 10, 100, 1000$ (from left to right). Depending on V_0, machine precision is reached at different N. Furthermore this method does not suggest a divergence for a high number of lattice points N and maintains machine precision.

Chapter 5

Application II: Coulomb Potential

5.1 Hydrogen Atom

Another example for a common 1D Schrödinger equation is radial equation of a particle in a Coulomb potential. As an example, the hydrogen atom will be examined.

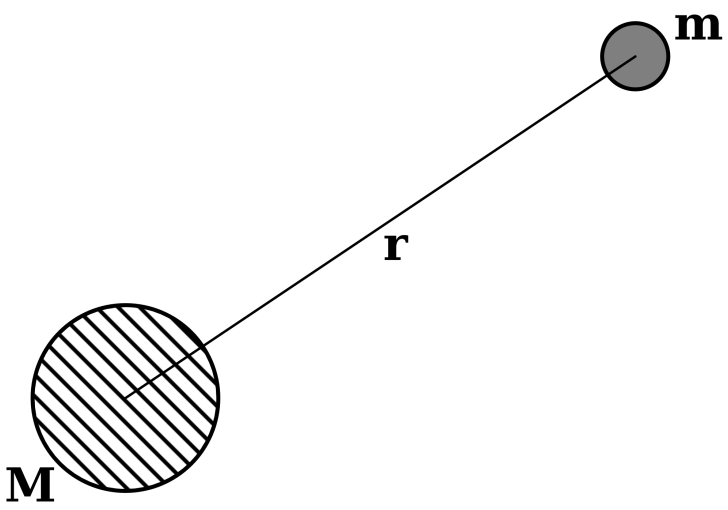

Figure 5.1: The hydrogen atom

The positively charged nucleus and the negatively charged electron are attracted via the Coulomb potential

$$V(r) = -\frac{Ze^2}{4\pi\varepsilon_0 r}, \tag{5.1}$$

which only depends on the distance r between them. The above formula is valid for all hydrogen-like atoms. Since we will examine the hydrogen atom in the following section, we set Z=1. In order to describe the system by the movement of the electron alone, we neglect the movement of the much heavier nucleus.

This yields the Hamiltonian

$$H = -\frac{\hbar^2}{2m}\nabla^2 - \frac{e^2}{4\pi\varepsilon_0 r} \tag{5.2}$$

Inserting the three dimensional Laplace operator in polar coordinates ∇^2 and separating the Schrödinger equation into a radial and an angular part yields the radial equation

$$\left\{\frac{\hbar^2}{2m}\left[\frac{1}{r^2}\frac{\partial}{\partial r}\left(r^2\frac{\partial}{\partial r}\right)\right] + \frac{\hbar^2}{2m}\frac{l(l+1)}{r^2} - \frac{e^2}{4\pi\varepsilon_0 r}\right\} R_{n,l}(r) = E R_{n,l}(r) \tag{5.3}$$

which under the transformation $u_{n,l}(r) = rR_{n,l}(r)$ simplifies to

$$\left\{-\frac{\hbar^2}{2m}\frac{\partial^2}{\partial r^2} + \frac{\hbar^2}{2m}\frac{l(l+1)}{r^2} - \frac{e^2}{4\pi\varepsilon_0 r}\right\} u_{n,l}(r) = E u_{n,l}(r). \tag{5.4}$$

Most commonly the effective potential

$$V_{eff}(r) = \frac{\hbar^2}{2m}\frac{l(l+1)}{r^2} - \frac{e^2}{4\pi\varepsilon_0 r} \tag{5.5}$$

is defined here, leading to the equation

$$\left\{-\frac{\hbar^2}{2m}\frac{\partial^2}{\partial r^2} + V_{eff}(r)\right\} u_{n,l}(r) = E u_{n,l}(r) \tag{5.6}$$

with the additional condition $u(0) = 0$.

5.2 Calculation of Exact Solutions

Because the exact eigenenergies of the hydrogen atom are known to be

$$E_n = -\frac{me^4}{8\varepsilon_0 h^2}\frac{1}{n^2}, \tag{5.7}$$

where n denotes the principal quantum number, the numerical solutions can be evaluated based on them.

5.3 Numerical Evaluation

As in Ch. 4, we calculate the ground-state energy with each method and examine how the relative differences between the exact and the numerical solutions behave when increasing N.

Defining a real space grid for the Coulomb potential is more difficult than

for the cosine potential since we have to select its length $L = Na$ ourselves. To account for the divergence of the Coulomb potential, we intentionally exclude the first point at $x = 0$. The interval has to be large enough to contain the ground state wave function $R_{10}(r)$. Since the Coulomb potential of the ground state falls off with $\propto 1/r$, the values at most grid points is close to zero. Therefore a higher number of lattice points is required to ensure a sufficient number of points in the relevant regime of the potential.

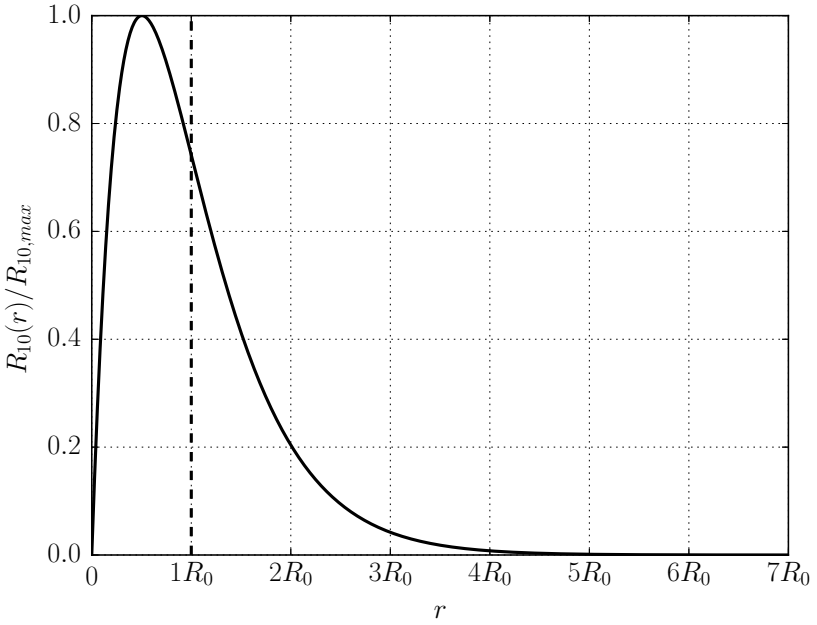

Figure 5.2: Ground state wave function $R_{10} = 2ra_0^{-\frac{3}{2}} \exp(-r/a_0)$. The used real space includes seven times the classical inversion point $R_0 \approx 1.05\mathring{A}$ illustrated by the dashed line

We set the length of real space as a multiple of the classical inversion point of the ground state R_0. This point is reached once the potential energy equals the energy of the state. Solving

$$E_{1,0} = E_{kin} + E_{pot} = 0 - \frac{e^2}{4\pi\varepsilon_0 R_0} \tag{5.8}$$

for R_0 and plugging in the ground state energy Eq. (5.7) with $n = 1$ yields $R_0 \approx 1.05\mathring{A}$. We chose $L = 7R_0$ and use a number of lattice points approximately ten times higher than for the cosine potential. Since all matrices are sufficiently sparse again, we use `scipy.sparse.linalg.eigsh` for the determination of eigenvalues.

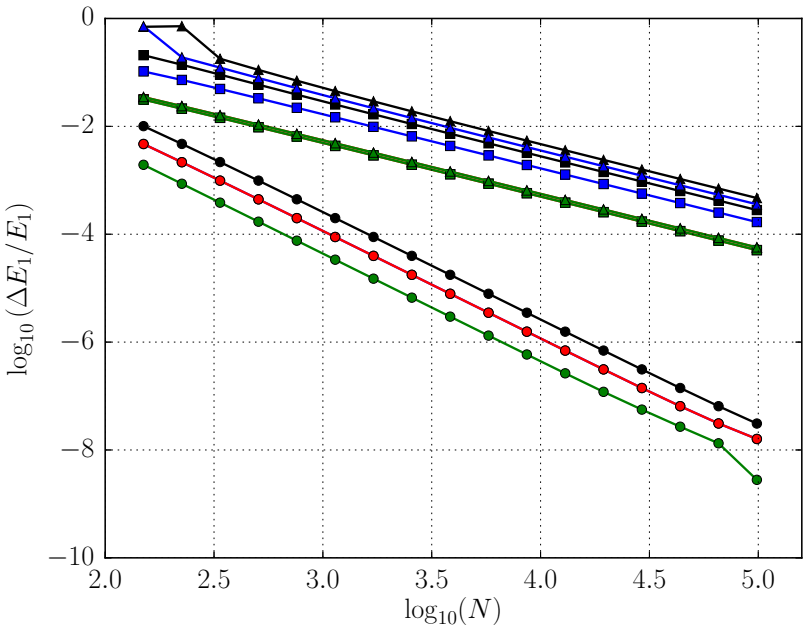

Figure 5.3: Comparison of all 4 solving methods by calculation of the ground state energy E_1 with $r = 1(\bigcirc), 3(\square), 5(\triangle)$. Green: standard matrix method; Red: matrix-Numerov method; Blue: alternative matrix method; Black: alternative matrix method with divergence.

In this case, a rather different behavior can be observed. First of all, despite the higher number of lattice points N, much less precise results are achieved. Therefore none of the methods reach a point where they enter a regime where instability occurs. A second difference is the superiority of first order methods in terms of both initial precision and rate of improvement. Since the theory cannot provide an explanation for this, presumably there is an underlying effect dominating over what is actually relevant.

Most likely the real space grid we defined causes complications, which increase for higher order approximations. Therefore, even though all methods find the ground state energy, the relative differences between them are distorted in a way, that does not allow a meaningful comparison.

Chapter 6

Conclusion

Since the results of the cosine potential agree with the theory and are much more precise than those provided by the evaluation of the hydrogen atom, we assume that only the cosine case helps to reconstruct the actual behavior of the matrix methods. In case of the hydrogen atom, underlying effects seem to dominate in a way that the insight gained form this application is very limited. Thus only the data from the cosine potential helps us understand stability and overall viability of each solving method.

According to the first application's results, all four matrix methods show signs of instability for $r > 1$, since they all seem to be confined by a linear function discussed in Sec. 4.3. Therefore when applied, one has to keep in mind that increasing the number of real space lattice points might worsen the precision of the generated eigenenergies. Using a reasonable number of lattice points $N \in [100, 10000]$ still provides good results, which depending on the used method can almost reach machine precision.

In a direct comparison the matrix-Numerov method is better than the standard matrix method as the theory suggests. However, the alternative matrix method without divergence explained in Sec. 3.3 appears to be the best of the four methods.
Regardless, solving the cosine problem in momentum basis provides such exact and entirely stable results that this method is to be considered superior over all others. Since it converges exponentially in opposition to all four other methods, it presumably is the best option for periodic potentials in general.

Because the hydrogen atom did not provide any useful data, we cannot be certain, what the general behavior of the algorithms is. Some of the effects showcased here could be caused by the periodicity of the cosine potential.

Chapter 7

Appendix

7.1 Shooting Method with Numerov's Trick

As described in Sec. 2.4, a Runge-Kutta method can be derived through the discretized second-order derivative with Numerov's trick very similarly. Plugging Eq. 2.16 into Eq. 2.17 yields

$$\begin{aligned}\psi_{(i+r)} = &\left\{\frac{c_r}{a^2} + kd_r\left[E - V_{(i+r)}\right]\right\}^{-1} \\ &\times \left[2\left[V_i - E\right]\psi_i - \sum_{j=-r}^{r-1}\left[\frac{c_j}{a^2} + kd_j\left(E - V_{(i+j)}\right)\right]\psi_{(i+j)}\right]\end{aligned} \tag{7.1}$$

for any $r > 0$. Because the number of adjacent wave function points necessary for the calculation of each value of the second-order derivative is equal under the usage of Numerov's trick, from here on the whole procedure is the same as in Sec. 2.4. Analogously to Tab. 2.1 the Runge-Kutta method with Numerov's trick for $r = 1$ yields

N	200	400	800	1600	3200	6400
$\Delta E_1/E_1$	1.01e-02	5.04e-03	2.48e-03	1.23e-03	6.47e-04	2.81e-04

Table 7.1: Relative errors of ground state energy $\Delta E_1/E_1 = \left|E_1 - E^{(c)}\right|/E_1$ calculated with the bisection Alg. 1 for different numbers of lattice points N. The Numerov-improved version of the discretized second-order derivative is used for the Runge-Kutta method. Again, a higher number of lattice points results in a direct improvement of the result.

Bibliography

[1] Mohandas Pillai, Joshua Goglio, and Thad G. Walker. *Matrix Numerov Method for Solving Schrödinger's Equation.* Department of Physics, University of Wisconsin-Madison, June 2012

[2] D. Tang. *B.Sc. Thesis.* National University of Singapore, 2014

[3] Lisa Arndt. *Numerov's Method.* RWTH Aachen, April 2017

[4] J. Ulrich and F. Hassler. *Dual approach to circuit quantization using loop charges.* Phys. Rev. Lett. **94**, 094505, 2016.

[5] John M. Blatt. *Practical Points Concerning the Solution of the Schrödinger Equation.* Hebrew University, Jerusalem, 1967

[6] Anders W. Sandvik. *Numerical Solutions of the Schrödinger Equation.* PY 502. Boston University, 2016

[7] J. Koch, T.M. Yu, J. Gambetta, A.A. Houck, D.I. Schuster, J. Majer, A. Blais, M.H. Devoret, S.M. Girvin, R.J. Schoelkopf. *Charge insensitive qubit design derived from the Cooper pair box.* Yale University and Universit de Sherbrooke, September 2007

Ich versichere, dass ich die vorliegende Arbeit selbstständig verfasst und keine anderen als die angegebenen Quellen und Hilfsmittel benutzt sowie Zitate kenntlich gemacht habe.

Ole Jasper	Datum